Proceedings of ASME Turbo Expo 2019:
Turbomachinery Technical Conference and Exposition
GT2019
June 17-21, 2019, Phoenix, Arizona, USA

GT2019-90394

VALIDATION OF A NEW TURBULENT FLAME SPEED FACILITY FOR THE STUDY OF GAS TURBINE FUEL BLENDS AT ELEVATED PRESSURE

Anibal Morones, Mattias A. Turner, Victor León, Kyle Ruehle, Eric L. Petersen
J. Mike Walker '66 Department of Mechanical Engineering, Texas A&M University
College Station, TX, USA

ABSTRACT

Turbulent combustion is a very active and challenging research topic of direct interest to the design and operation of gas turbine engines. A spherically expanding flame immersed in a turbulent field is one way to gain fundamental insight on the effect of turbulence on combustion. This kind of experiment is often conducted inside a fan-stirred flame bomb, preferably at conditions of high pressure, high temperature, and intense turbulence. A new fan-stirred flame bomb was designed and built to provide a device for conducting fundamental turbulent flame measurements at conditions of interest to gas turbine engines. A literature review on existing systems was used as guidance in the design of the turbulence-generation elements in the present rig. A few options of impellers were explored. The flow field produced by the chosen impeller was measured with Laser Doppler Velocimetry (LDV). A detailed exposition of the vessel engineering and construction are presented, including current activities that will extend the use of the facility for heated experiments up to at least 400 K. Before turbulent experiments were attempted, a validation of the rig accuracy and pressure worthiness was made. Finally, a demonstration of the new apparatus was made by testing a lean mixture of syngas. The experiment matrix using hydrogen and H_2/CO mixtures included three levels of pressure (1, 5, and, 10 bar) and three levels of turbulence fluctuation rms (1.4, 2.8, and 5.5 m/s). Data based on the high-speed schlieren diagnostic are presented.

INTRODUCTION

The rigorous study of the effect of turbulence in combustion is fairly recent [1] despite the length of time that combustion science has existed as a major field of reseach. In his seminal work, Damköhler offered a few reasons for this tardiness: the lack of a quantitative description of turbulence, which only existed for one simple case at the time; and the disconnect between the communities interested in the study of combustion and turbulence. Damköhler insisted that any attempt to comprehend the effect of turbulence on flame propagation must start with numerical data on the turbulence.

While there is significant progress on the understanding of fundamental aspects of turbulent combustion and the underlying physical constitutive relations are known, namely, conservation of species, mass, energy, and momentum, the sheer number of scales and species to be solved is computationally prohibitive for the foreseeable future [2]. There is now a sizeable portion of the combustion research community working to develop predictive models that can handle relatively unstudied chemical compositions at high pressures and Reynolds numbers [3].

The development of models from canonical flames and idealized laboratory conditions may take longer to impact the technology of practical applications, as opposed to those efforts channeled to improve the performance of a specific device. However, simpler experiments that are amenable for both meticulous measurements and high-fidelity modeling provide a more sound approach to build fundamental understanding [4]. The search of a better understanding of turbulent combustion is not driven by purely academic interests. Environmental concerns and resource depletion, among other factors, are pushing combustion applications to improve performance while reducing pollutant emission. A better understanding of turbulent combustion could help to cope with this exigence.

Spherical flame experiments can support the advance of turbulent combustion science by producing measurements for conditions and species that are outside the borders of current numerical simulation capabilities or for which little is known in the literature. Worldwide, there are few fan-stirred flame vessels that are capable of testing conditions higher than ambient temperature and pressure and that are also able to produce turbulent flow fields that are relevant to practical devices. Table 1 offers a summary of the devices found in the literature, and Fig. 1 displays the variety of shapes and sizes encountered in fan-stirred flame bombs [5-24]. Figure 2 summarizes the three main capabilities—temperature, pressure, and velocity fluctuation—on a 3-D plot.

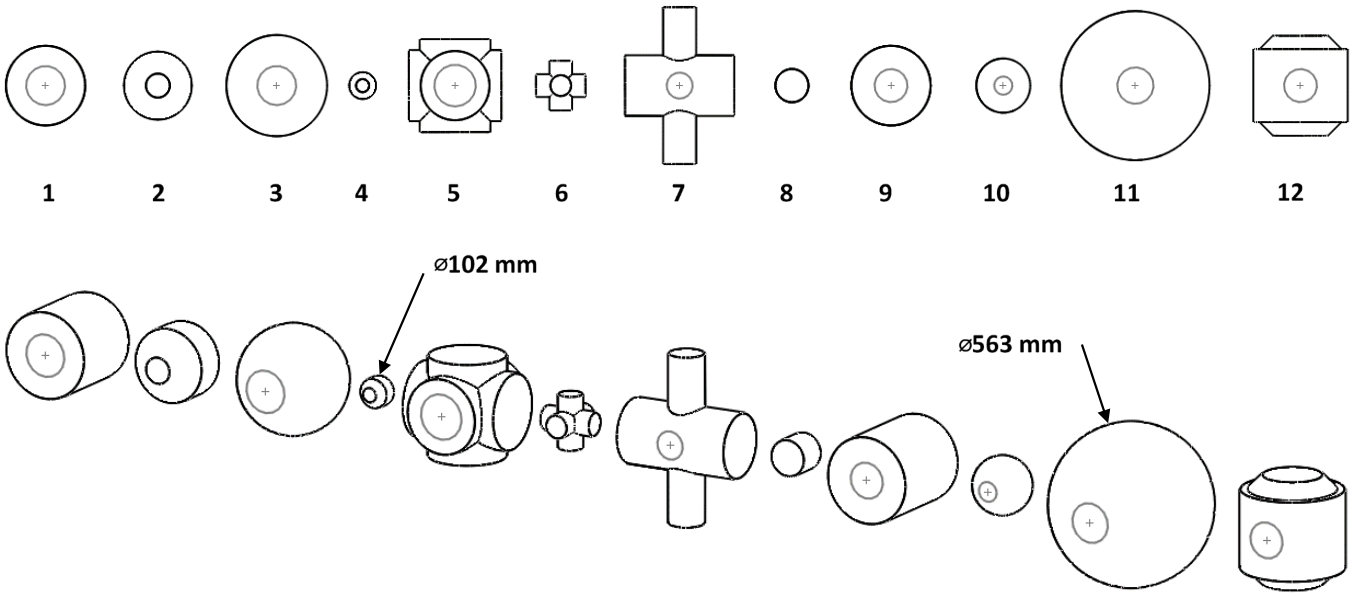

Figure 1. Interior volume of fan-stirred flame bombs. The ID number matches the order listed in Table 1.

Table 1. Fan-stirred flame vessel literature survey.

ID	Institution	Format & dimensions mm	volume liters	Max. temp. K	Max. press. bar	Turb. rms m/s
1	U Leeds 1st gen. [5]	Cylinder ⌀ 305, L 305	22.3	300	1	16
2	GM/UMI [6-8]	Spheroid ⌀ 260, L 265	10.6	300	5	2.5
3	U Leeds 2nd gen. [9]	Sphere ⌀ 380	28.73	600	15	11.9
4	UMI [10]	Spheroid ⌀ 102	0.8	300	1	1.8
5	Kyushu U [11,12]	3 intersecting cylinders ⌀ 265	35.0	300	10	3.2
6	KIT [13,14]	3 intersecting cylinders ⌀ 80, L 190	2.28	300	70	3.5
7	Taiwan NCU [15-18]	Cruciform ⌀ 120, 245, L 600, 420	26.6	300	10	8.3
8	Princeton [19,20]	Cylinder ⌀ 114, L 127	1.29	300	30	6.0
9	TAMU 1st gen. [21,22]	Cylinder ⌀ 305, L 356	25.9	300	1	1.5
10	U d'Orléans [23]	Sphere ⌀ 200	4.2	473	10	2.8
11	CNRS-ICARE [24]	Sphere ⌀ 563	93.4	573	20	3.7
12	This work	Spheroid ⌀ 356, L 406	33.8	473	10	5.5

Inspection of the literature review results in Table 1 and Figs. 1 and 2 highlight the areas that are well covered and those that are less covered in terms of experimental conditions. For example, there are vessels that can indeed operate at elevated pressure, with at least 8 facilities that can handle test pressures of at least 5 bar. Fewer vessels can be operated at pressures greater than 10 bar, however. An extreme example is the rig built by Weiß machined out of a single piece of steel that can operate up to 70 bar (#6 in Table 1) [13,14]. Some others, at least 3, can withstand temperatures above ambient and are suitable for the study of liquid fuels. Few can stir with a turbulence fluctuation rms greater than 5 m/s. Only one facility combines all three capabilities and stands out in green in Fig. 2 (#3 in Table 1), this being the 2nd generation vessel from the University of Leeds [9].

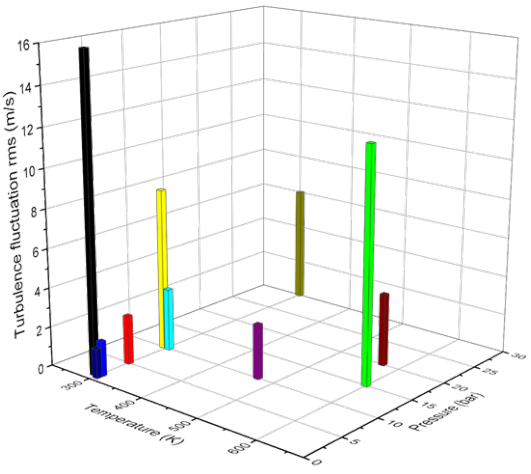

Figure 2. Domain of operating conditions of flame bombs listed in Table 1. Note that the entry of KIT has 70-bar capability (not shown here).

The primary objective of the present work was to design and build a fan-stirred flame bomb for the study of turbulent combustion at elevated pressure and temperature. Such a device and related experiments are relevant to gas turbine engine combustors in several ways. First, turbulent flame speeds and other details can be studied at fundamental conditions that overlap with those of interest to gas turbine engines (u′, length scale, pressure, temperature, mixture, etc.). Second, a carefully controlled experiment such as the one presented herein can be used to generate data from well-characterized initial and boundary conditions; such data can then use used to validate numerical models of the turbulent combustion process. These models can then be used perform turbine-relevant simulations with higher confidence. Third, the data obtained from the present rig will provide fundamental knowledge and insight on turbulent flames. This insight can be used for trend prediction and general understanding of turbulent flames at engine conditions.

Within this paper, a detailed description of the new device design is provided first. Characterization tests are described next. Then, a validation study using a syngas fuel blend is presented to demonstrate the capabilities of the newly implemented device. The results are then discussed.

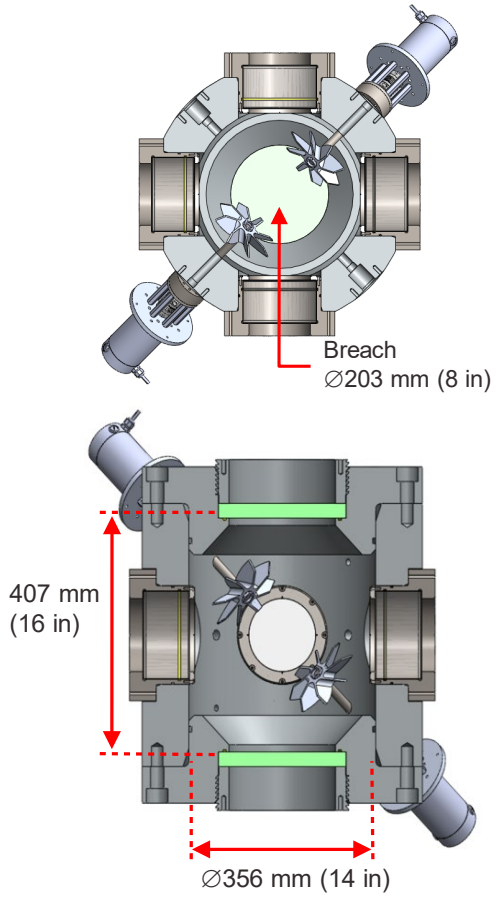

Figure 3. Schematic of the fan-stirred flame speed vessel design.

FACILITY DETAILS

A new, high-pressure turbulent flame speed rig was designed and set up in the authors' laboratory. The final design has a tetrahedral fan orientation, as shown in the cutaway in Fig. 3. The cylindrical vessel has an inner diameter of 35.6 cm and an internal length of 40.7 cm. The window-aperture-to-ID ratio is 36%. Provided in Fig. 4 is a photograph of the finished rig in place within the test cell, and Table 2 summarizes the key dimensions and specifications. Provided in this section are brief overviews of the main hardware assemblies on the rig. Further details can be found in the thesis of Morones Ruelas [26] and in Morones et al. [27].

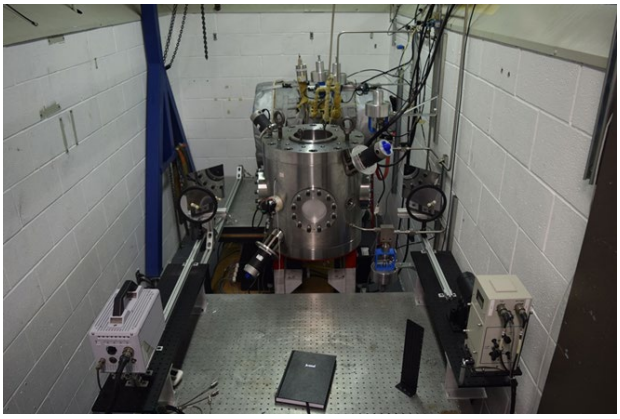

Figure 4. Test cell layout at Texas A&M University. The fan-stirred flame vessel of the present work is at center.

Table 2. Turbulent flame speed vessel key values [27].

Target Metric	Value
Window opening	127 mm
Breach opening	203.2 mm
Maximum pressure* †	10 atm
Maximum temperature*	150 °C
Turbulence fluctuation rms	10 m/s
Turbulence int. length scale	30-50 mm
Maximum impeller diameter	178 mm
Maximum speed	10,000 rpm
Internal diameter	355.6 mm
Internal vessel length	406.7 mm

* Prior to ignition.
† Without venting. Vessel operating as closed volume.

Fan-Stirring Assembly

The study of other facilities from the literature and their stirring fans showed that the impeller should be larger than previously attempted in the first generation of fan-stirred flame bombs at Texas A&M University [21]. There are of course limitations on how large the impeller can be to produce a certain fluctuating velocity for a given motor speed and power

consumption, as shown in Morones et al. [27]. Also, the impeller should preferably be small enough to fit through the vessel window bore to facilitate assembly, i.e. $\varnothing \leq 17.14$ cm.

Five impeller designs of similar diameter were evaluated. Four different designs were custom made for this study using rapid prototyping, and their geometries and dimensions are shown in Fig. 5. The fifth stirrer was a commercial leaf blower/vacuum impeller, Toro 127-7092. The blower impeller is made of magnesium and has backward-curved blades. Its diameter is 12.4 cm, and the axial length is 5 cm. The resulting internal velocity map was characterized for each fan type using a Laser Doppler Velocimetry (LDV) diagnostic over a range of fan speeds from 0 to 6000 rpm. Details of the velocity characterization can be found elsewhere [26]. The end result was that the commercial leaf blower fan provided the most homogeneous flow field.

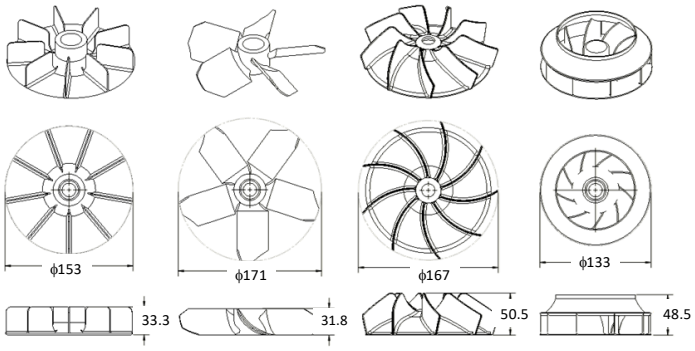

Figure 5. Custom impeller prototypes tested. From left to right: radial, axial, backward curved, plug design. Dimensions are in mm.

Fan-stirred flame vessels aspire to produce a region of isotropic, homogenous turbulence with negligible mean flow. The unbalance between the horizontal and vertical components of the turbulence fluctuation is therefore unfavorable. Fortunately, this kind of cylindrical apparatus with tetrahedral fan configuration (Fig. 3) can adjust the relative importance of the horizontal and vertical rms values by sliding the impeller along the shaft closer or away from bomb center, Fig. 6. As the blades come closer to the vessel wall, the later acts as a shroud or housing that favors the flow along the cylindrical axis.

Stirring the contents of a pressure vessel with fans is not a trivial task. A penetration into the pressure vessel must be made to drive the shafts, which have seals that allow the best possible control of the composition of the gaseous mixture inside the vessel without leaking and also that consistently survives the overpressure of a confined deflagration. In addition, the stirring assembly is expected to run at a maximum speed of 10,000 rpm at temperatures above ambient.

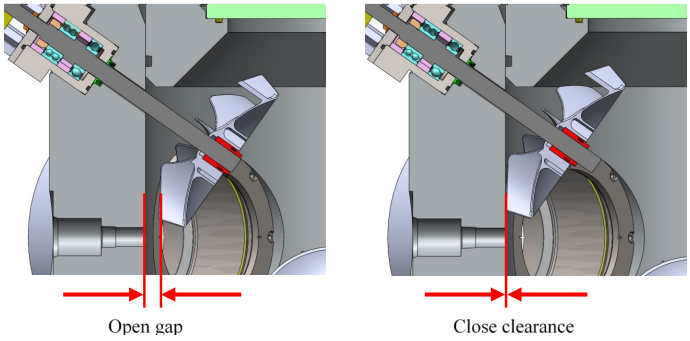

Figure 6. Comparison of impeller installation position. On the left, the impeller is installed at the tip of the shaft, closest to the center. On the right, the impeller has only a small clearance with the cylindrical wall.

The selection of the motor was constrained to a number of factors such as power demand, ease of assembly, maintenance and operation. During design, it was decided to mount the motor directly on the vessel. The motor had to be strong enough to drive the fan and overcome the seal friction while being light enough to be easily handled by one person and flange-mounted directly on the apparatus. The primary author decided to motorize the shaft with two different motors to cover the range of desired speed. To run in low range, from 0 to 6000 rpm, a DC-brushed motor was chosen. The DC motor main characteristics are listed in Table 3. The DC motor is nominally rated 323 W (0.429 hp), although it can handle overloads for short periods of time. The DC motor control, KB Electronics model KBMD-240D, was upgraded with a heatsink to increase the deliver up to 745.7 W (1 hp).

Table 3. Technical specifications of the Ametek Pittman ID33005 DC-brushed motor.

Specification		
Supply Voltage	90	Vdc
Continuous Stall Torque	0.85	N-m
Speed @ Cont. Torque	6000	rpm
Current @ Cont. Torque	8.33	A
Continuous Output Power	323	W
	(0.429	hp)
Maximum speed	6000	rpm
Peak Current	33.20	A
Peak Torque	4.24	N-m
Weight	3.27	kg

The higher end of the speed range, 8,000 - 10,000 rpm, is powered with a router motor pack. The motor pack has a built-in speed controller that allows for adjusting the rotational speed from 8,000 to 24,000 rpm, albeit not very precisely. A fixed router base permits a convenient coupling with the receiving flange of the stirring assembly.

The fan shaft was designed to a maximum speed of 10,000 rpm. The critical speed was estimated with the Rayleigh–Ritz method. The fan weight was modeled as a lump load applied at the tip of the shaft. The shaft was approximated as a cantilever beam 16.5 cm long in the analysis, which corresponds to the distance from the guide bearing to the shaft tip.

A hammer impact test was performed to a stirring assembly, and the natural frequency acquired was 176 Hz with the impeller installed at the tip of the shaft. This result corresponds to a critical speed of 10,560 rpm, which confirms that the approximations taken for the Rayleigh–Ritz calculation were reasonable. A different configuration, with the leaf blower installed with a close clearance the bomb interior wall (Fig. 7), produced a natural frequency of 448 Hz. The alternative fan location critical speed, 26,880 rpm, is much higher and well away from the operation range of the stirring assembly (10,000 rpm).

During the design phase, the shaft was opted to be machined without keyways. Balanced-keyless torque couplings, adapters, and locknuts were chosen. This decision produces a rotating assembly that is balanced from design and also provides flexibility regarding the relative location of the shaft coupling and impeller along the shaft. This flexibility is needed because the fan shaft is to be connected with at least two different motors and possibly several different impellers. While the motors were chosen to have the same shaft diameter, so that a single coupling could be used for both, their shaft lengths are not identical. Figure 7 shows a detail of the impeller and shaft coupling. The bellows coupling can be slid to facilitate assembly, colored yellow in the assembly cross section of Fig. 7. With the proper machining tolerances, keyless shaft-hub connector provides a very secure interference fitting with the impeller at any position along the shaft. The keyless connector has been colored bright red in the assembly view, Fig. 7.

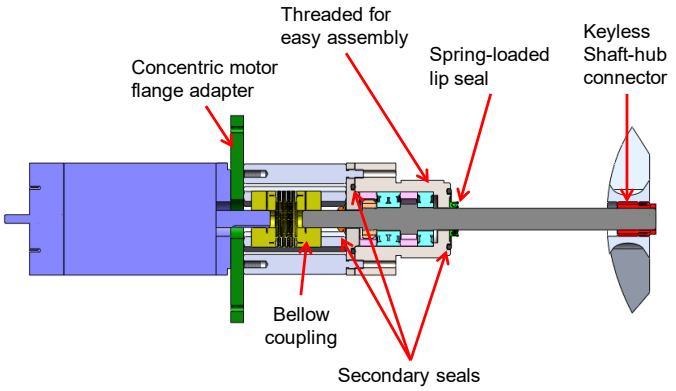

Figure 7. Schematic view of the impeller and shaft coupling and entire assembly.

The primary seal around the shaft and the vessel penetration is a spring-loaded PTFE lip seal, shown in bright green in Fig. 8. The lip seal has a flanged profile that is clamped between the vessel body and the bearing housing to ensure that the seal does not spin with the shaft. The lip seal material is chemically inert at elevated temperatures and pressures and is capable of running without lubrication at high surface speeds. It is rated for 20.6 MPa (3,000 psi) at maximum rotary surface speed of 1,500 ft/min. The shaft was ground to surface finish of R_a 0.15 µm as recommended by the seal manufacturer. Secondary containment seals have been placed in tandem. A pair of o-rings closes the static path, while a v-ring, orange in Fig. 8, keeps contaminants out of the bearing cavity and weakly assists vacuum seal.

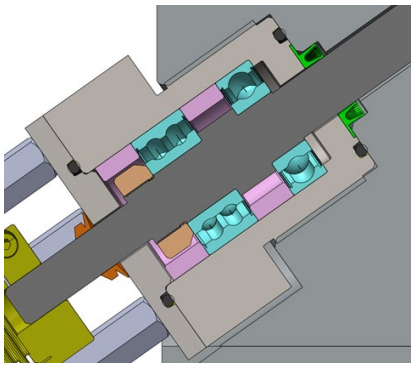

Figure 8. Vessel wall and stirring assembly detailed cross section.

A cage is created with six standoff bolts that serve multiple purposes as they secure the bearing housing lid, enclose the shaft coupling, and provide a mounting structure for the motor receiving flange. The concentric design makes a robust assembly because the maximum possible misalignment of the shafts is limited by the clearance and machining tolerances. Nevertheless, the metal bellows coupling absorbs and accommodates any leftover misalignment.

Windows and Schlieren Setup

Two sets of orthogonal windows is a key feature of this apparatus. Orthogonal lines-of-sight enable optical techniques that potentially resolve the 3D structure of the flame in tomography or even stereoscopy, as opposed to the 2-D projection of schlieren imaging. For example, the instantaneous flow field at a given cross section can be rendered using PIV, or the concentration of a specific species can be mapped across the flame at any time applying planar laser induced fluorescence.

The window substrate is padded with 0.8-mm thick PTFE gaskets and is gently clamped inside the cell. The clamp does not need to be very strong because its function is to retain the substrate in place in vacuum. A couple of circumferential o-rings shut the gas path. The o-ring glands are highlighted in yellow in Fig. 9. This arrangement makes the viewport airtight and keeps the window in a low-stress state.

A maximum pressure of 20.6 MPa was used to design the window thickness using a combination of hand calculations and finite element stress analysis. A 7.6 safety factor was chosen, exacting a minimum thickness of 8.9 cm. Simulations show an

overall low-level stress with a maximum tension stress of 15.8 MPa (2.3 ksi) on the center of the exterior face when an internal pressure of 20.6 MPa is applied, as detailed in the thesis of Morones [26].

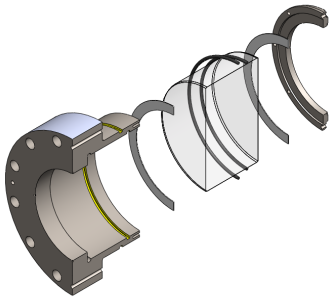

Figure 9. Exploded cutaway view of the window subassembly.

For the demonstration experiments of turbulent flames presented herein, a schlieren diagnostic setup was used to visualize the flame propagation. Figure 10 shows the basic setup for the new rig when using a z-type setup arrangement with focusing mirrors. An alternate configuration using flat mirrors and focusing lenses can be employed as well; this latter style is visible in the rig photograph in Fig. 3.

Pressure Vessel and Fasteners

In its present configuration, the vessel is intended to perform spherical flame experiments with a pressure up to 10 atm prior to ignition. An instantaneous peak pressure of roughly 10 times the initial pressure is typically expected in closed-volume combustion. Therefore, the design maximum pressure was chosen to be 100 atm (1,469.6 psi). To accommodate such a pressure and for ease of manufacture, the material chosen for this apparatus was forged martensitic stainless steel. The ASTM grade specification in its hardened condition is A182 F 6A Class 4. The material was shaped into seamless rings. The construction of the pressure vessel out of forged cylinders eliminated welding procedures.

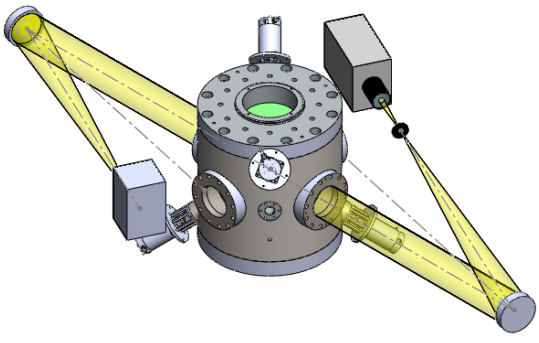

Figure 10. Typical schlieren configuration for the new rig, showing the light source (bottom left), 2 focusing mirrors, and camera (top right); z-type configuration shown here.

Using standard pressure vessel relations, the minimum cylinder thicknesses found for circumferential stress and longitudinal stress were 10.0 mm and 4.8 mm, respectively. The vessel was built with a wall thickness of 8.9 cm, which yields a safety factor of 8.9. The minimum thickness of un-stayed flat heads, cover plates, and blind flanges were designed to conform to the requirements given in the ASME Pressure Vessel Code, Section VIII UG-34 [28].

The endcap does not have a constant cross section; it is thinnest at the bolt flange, 6.35 cm, and much thicker around the retaining ring thread and vent opening. Analysis produced a safety factor of 1.63 for the endcap design. The highest stress areas are very localized and limited to the fillet between the bolt flange and the cylindrical projection that is inserted into the bomb body [26]. For this reason, the fillet radius was generously sized to 10.2 mm, which make it the largest fillet feature among all the vessel components.

Selection and design of the fasteners were done following the guidelines of the *Machinery's Handbook* [29]. The typical bolt strength is 1168 MPa (170 ksi). For the minimum engagement length, the fact that the internal threads are machined into the forged stainless steel with a lower strength had to be considered. The forged ring's strength is 756 MPa (110 ksi), and the engagement length was corrected so that the bolt would fail before the internal threads would strip. The minimum engagement requirement was relaxed in the case of the bearing housing thread since it has a very generous safety factor.

The endcaps have a 20.3-cm-diameter breech and retaining ring. The retaining ring holds in place accessories fitted at the breech, of which the simplest option is a plug blank, as presented in Fig. 11. The thread chosen for these elements is a standard 10-3 BUTT 3A buttress screw, known for being particularly strong in one direction. A breech design was employed so that the vessel in the future could be extended to include a burst disk (blank plug in Fig. 11) that will fail during an experiment and hence allow the pressurized gases to quickly escape. Operating in this vented fashion will extend the test pressure capability of the present rig to 20 atm.

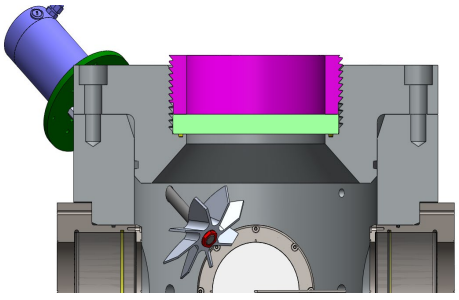

Figure 11. Detail cutaway showing the retaining ring in magenta and a blank plug disk in light green.

Heating System

Development of an internal heating system for the turbulent flame speed vessel is currently in progress to control the initial temperature of a flame test. Current heating methods heat the entire mass of the vessel, as in Krejci et al. [26], and therefore require a significant amount of time to reach the target temperature of 150°C. This new system will only heat the gas mixture inside the vessel rather than the entire vessel itself, reducing total heating time. Two 500-W resistive heaters, controlled by a thermostat, are secured within the vessel prior to testing. Uniformity of the resulting gas mixture within the vessel was verified with thermocouples. In a typical fame speed experiment, the vessel is filled with the test gas mixture, heated for approximately 20 minutes, and then ignited.

During the initial characterization of the first-generation heating system design, it was found that the gas mixture loses heat to the vessel wall too rapidly. Adhesive ceramic fiber insulation adhered to the internal wall allowed the gas mixture to reach target temperatures, but it created too much dust during turbulent flame speed tests. An improved insulation method is currently under development.

Rig Validation and Characterization

A hydrostatic test was performed on the finished vessel by FESCO, Ltd. The vessel was filled with water and then pressurized 13.7 MPa (2,000 psi) with a pneumatic pump. No leaks or pressure loss were observed, however, one quartz window fractured. Even in its broken state, the window did not disintegrate; it continued to hold pressure without releasing water. The hydrostatic test was considered successful as the worthiness of the vessel was verified. As a corrective measure, PTFE gaskets were added to the window assembly to avoid direct contact between metal and quartz on the flat faces and minimize stress concentration, as shown in Fig. 9.

Since this is a new device, a validation diligence was necessary. A series of experiments with hydrogen was chosen as a figure of merit. Laminar flame speed experiments were performed for this validation (i.e., without the fan-stirrer assemblies). Using H_2-air mixtures at 1 atm, the vessel was able to reproduce results obtained in the past by this group [25] with excellent repeatability, Fig. 12.

However, the maximum operating pressure is 10 atm. The competence of the bomb under static load was judged with the hydrostatic test mentioned above. A conservative rule of thumb estimates that the pegging pressure, i.e. the momentary, peak pressure, will be tenfold the initial pressure for closed-volume combustion. Before commissioning the bomb for operation at 10 atm, trial experiments with aluminum window plugs in place of the quartz windows were performed. The high-pressure trials with the aluminum window plugs were successful, and a sample pressure trace is shown in Fig. 13. The 10-atm tests were successfully repeated with the window cells again fitted with quartz substrates.

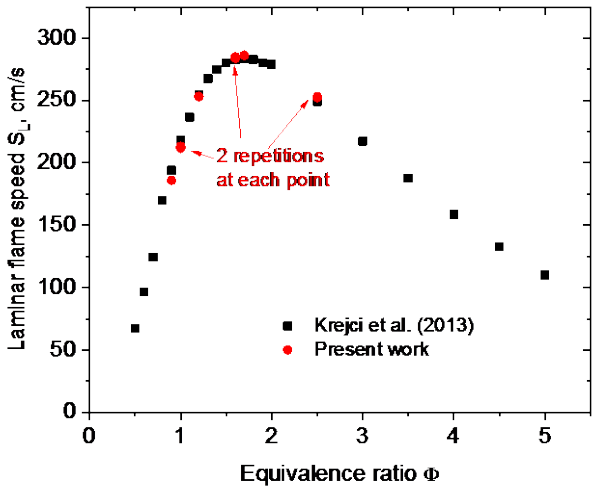

Figure 12. Laminar flame speed of hydrogen at 1 atm and room temperature from the present facility and compared with historical data from the authors' group [25].

It was noticed that, after the high-pressure experiments, the combustion products when seen through the window immediately after a run had a distinctively yellow/greenish coloration. The yellow shade was more intense the higher the initial pressure; in other words, combustion products of 10-bar experiments were decidedly mustard, while the coloration after 2-bar runs was barely perceptible. Moreover, if the combustion gases were allowed to sit in the vessel and cool down, the mustard hue faded away gradually. The water that eventually condensed inside the bomb had a bright yellow color, while some surfaces were stained with a dark brown/rust patina. To minimize condensation and the residue left behind, the combustion products were vented through the ventilation system as quickly as possible. Even with the extraction system working, a pungent, biting smell was perceived for a few seconds following the exhaust release.

It was postulated that the mustard coloration was owed to the formation of nitrogen oxides (NOx). The physical and chemical characteristics of nitrogen dioxide (NO_2) in particular fit the observations quite well, including the color. To test this hypothesis, a simple test was devised; to substitute nitrogen in the oxidizer for an inert gas: helium. A 10-atm run of hydrogen at an equivalence ratio of 0.5 was prepared with a mixture of oxygen and helium in the following volume ratio: O_2:He = 1:6. The resulting combustion products were odorless and colorless. The condensate was also transparent.

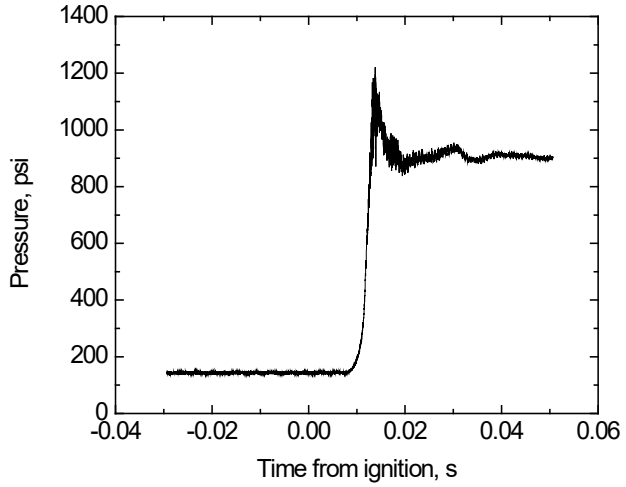

Figure 13. Pressure trace of a high-pressure experiment. Reactants pressure was 10 atm. Stoichiometric H_2-air.

After these tests, it was concluded that the coloration in the air-burning experiments was due to nitrogen oxidation. It can be said that, after the experiments, the bomb and the steam generated therein were acting as an unintended, wet scrubber. Nitrogen dioxide is highly soluble in water and decomposes in nitric acid promptly [30], which could explain why the gas-phase loses the yellow color if enough time were allowed, leaving a tarnished condensate behind.

Flame vessels are finite-volume devices, and therefore pressure is expected to increase after combustion takes place. However, in the early stages of the flame development, there is very little change in pressure. The current device demonstrated that the pressure increase during the time the flame is being recorded is negligible, see Fig. 14. This claim was later confirmed during the analysis of the images to obtain the laminar flame speeds. A confinement effect was also not observable in the burned velocity-versus-stretch plots. This lack of observed confinement effect might be due to the fact that this new chamber diameter and volume are greater than those employed in former generations of flame speed vessels at Texas A&M University [31,32].

SYNGAS DEMONSTRATION

To demonstrate operation of the new facility, experiments were performed for turbulent flames over a range of pressures. An equimolar mixture of H_2 and CO was chosen as a representative syngas blend. Provided in this section is a review of the test matrix and the experimental conditions, followed by representative results.

Test Matrix

The fuel chosen to demonstrate the capabilities of the new rig was a mixture of hydrogen and carbon monoxide in equal volumetric proportion. The effect of pressure on the laminar flame speed of this particular mixture has been previously studied by the authors' group [25]. Only one equivalence ratio was studied in the present work, $\phi = 0.5$. This mixture is the approximate air-fuel composition at which syngas is burned in stationary gas turbines [33]. The fans were operated at 2000, 4000, and 8000 rpm to induce corresponding planar turbulence fluctuations, u′, of 1.4, 2.8, and 5.5 m/s, respectively.

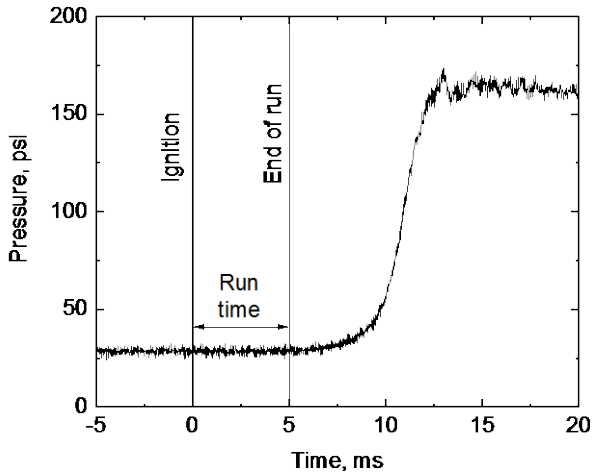

Figure 14. Pressure trace from a 2-atm H_2-air experiment. The flame silhouette reaches the edge of the field of view well before 5-ms mark, when the increase in pressure is not perceptible.

Three levels of pressure, 1, 5, and 10 bar were explored, but not all combinations of shaft speed and pressure were attainable. It was not possible to run experiments at 8000 rpm for 5- and 10-bar experiments. Both the motors and the current electrical installation proved to be insufficient to overcome the power demand imposed by the lip seal at high pressure. All experiments were conducted at room temperature. For the fans, the leaf blower impellers were placed near the wall.

Table 4 summarizes the laminar flame speed, flame thickness, and turbulent Reynolds number Re_T for the test matrix. The integral length scale of the turbulence, L_T, is typically derived from spatial correlations computed from instantaneous snapshots of the flow field. Particle Image Velocimetry (PIV) is the preferred tool for such analysis. Unfortunately, PIV measurements were not available for the present study, and L_T was assumed to be equal to the length of the leading edge of the impeller, i.e. 20 mm. The lack of information about the spatial coherence also prevented the spectral analysis of wavelengths. The spectral distribution could have been used to estimate the energy dissipation rate. A crude approximation to the energy dissipation rate can be obtained from the ratio of power taken from the electrical grid and the mass trapped in the bomb. The average energy dissipation rate must be less than such a

quotient since the motor and drive train power losses are unaccounted. From the velocity field characterization, the isotropy (u′/w′) for the conditions provided in Table 4 was 1.016 or better.

Table 4. Flame properties and Re of test mixture at ϕ = 0.5, L_T = 20 mm, T = 300 K. The 3 turbulent speeds shown correspond to fan speeds of 2000, 4000, and 8000 rpm, respectively.

	$S_{L,u}^{\circ}$	δ_∇	δ_α	$\mathrm{Re}_T = u'L_T/\nu$		
	m/s	µm	µm	1.4 m/s	2.8 m/s	5.5 m/s
1 bar	0.269	649	107	1621	3242	6369
5 bar	0.130	195	45	8116	16,231	
10 bar	0.081	142	36	16,185	32,370	

The laminar flame thickness has multiple definitions. The thermal diffusivity thickness, δ_α, shown in Eqn. (1), is derived from dimensional arguments as the ratio of the thermal diffusivity of the fresh reactants and laminar flame speed. This definition is not the only diffusive thickness, and some authors prefer to assess the flame thickness in terms of other transport properties. In fact, it is not uncommon for all transport properties to be assumed numerically equal in some derivations (i.e., $\alpha = D = \nu$). This treatment is implicit in the construction of Borghi diagrams, since curves of constant Reynolds number are shown as straight lines in the logarithmic space. The permute of momentum and thermal diffusivity is defensible for air in a wide range of temperatures as the Prandtl number (Pr) stays somewhat close to unity (Pr = $\nu/\alpha \sim 0.7$)) and allows for Eqn. (2) for the Reynolds number.

$$\delta_\alpha = \frac{\lambda_u}{\rho_u c_P S_L} = \frac{\alpha}{S_L} \tag{1}$$

$$\mathrm{Re}_T\big|_{\mathrm{Pr}=1} = \frac{u'L_i}{\delta_\alpha S_L} \tag{2}$$

Where λ_u (W/m^2-K) is the thermal conductivity of the reactants; S_L (m/s) is the laminar flame speed; ρ_u (kg/m^3) is the density of the reactants; c_p (kJ/kg-K) is the heat capacity at constant pressure; and α (m^2/s) is the thermal diffusivity.

Other definitions of the flame thickness are formulated from the temperature profile across the flame front. Figure 15 can be used to illustrate the temperature gradient thickness, δ_∇, which is obtained by extending a tangent line from the point of maximum slope to intersect the steady-state temperature line of reactants and products. This temperature gradient definition, expressed in Eqn. (3), is usually 5 times larger than the thermal diffusivity thickness (i.e. $\delta_\nabla \approx 5\,\delta_\alpha$) and is useful as a first approach to set the grid size in numerical simulations [34]. The total flame thickness, δ_{total}, which measures the distance needed by the combustion products to reach the final equilibrium temperature starting from the fresh gases temperature, is also depicted in Fig. 15.

$$\delta_\nabla = \frac{T_b - T_u}{\max\left(\left|\frac{dT}{dx}\right|\right)} \tag{3}$$

Where T_u is the temperature of the reactants; T_b is the equilibrium temperature of the combustion products; and x is the coordinate along the flame propagation. All conditions tested in this paper fall in the thin reaction zone as when represented on a Borghi diagram.

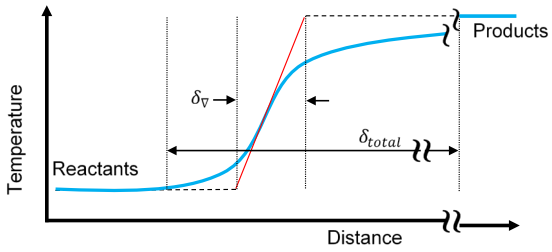

Figure 15. Mock temperature profile of a flame. The steepest rise and steady-state temperature of the products and reactants define the thermal gradient flame thickness, δ_∇. The total thickness, δ_{total}, is much larger.

Results and Discussion

A Photron high-speed camera, Fastcam SA1.1 was used to acquire schlieren images at 25,000 frames per second. Figure 16 provides sample images of turbulent flames at 1 bar for each of the three fan speeds. The still images were post-processed with an in-house Matlab script that finds the edge of the window and flame. The area-occupied flame silhouette is tallied, and the radius of a circle with the same area is calculated for every frame. With this information, it is possible to plot the equivalent flame radius over time. The radius development of three or four repetitions for each of the 3 fan speeds at 1 bar is displayed in Fig. 17. In all repetitions shown in Fig. 17, acceleration is noticeable as the flame grows. The stochastic nature of this phenomenon is manifested in the spread of repetitions, which is an indication of the repeatability of such turbulent flame measurements at a given initial condition. This behavior is in line with the observations of other research groups.

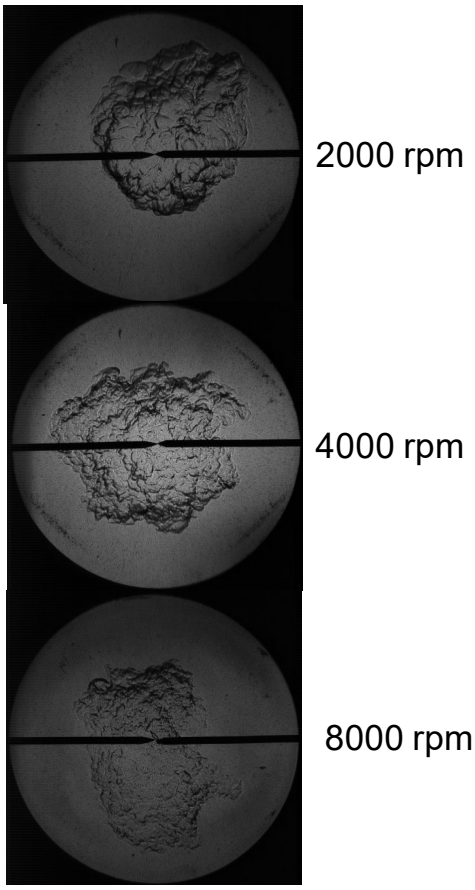

Figure 16. Typical schlieren images from 1-bar syngas flames for the three different fan speeds.

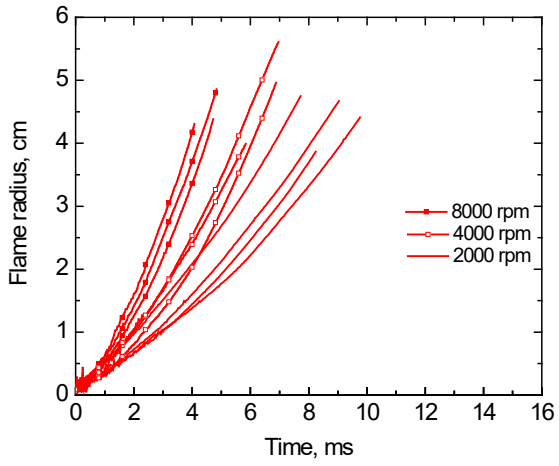

Figure 17. Radius histories of three (or four) test repetitions at 2000, 4000, and 8000 rpm and 1 bar.

Also seen in Fig. 17 is the effect of the fan speed on flame acceleration, which is larger than the scatter exhibited by the runs. Three distinct groups of curves can be observed for the 1-bar results. As expected, the faster the shaft speed the quicker the radius grows. Experiments at 2000 rpm presented slightly more scatter than those conducted at 4000 and 8000 rpm.

Presented in Figs. 18 and 19 are results for the 5-bar experiments at the two fan speeds of 2000 and 4000 rpm. Figures 20 and 21 show the results at 10 bar. The trends in these plots are similar to those seen for 1 bar, with higher growth rates noticeable for higher fan speeds (and turbulent intensities).

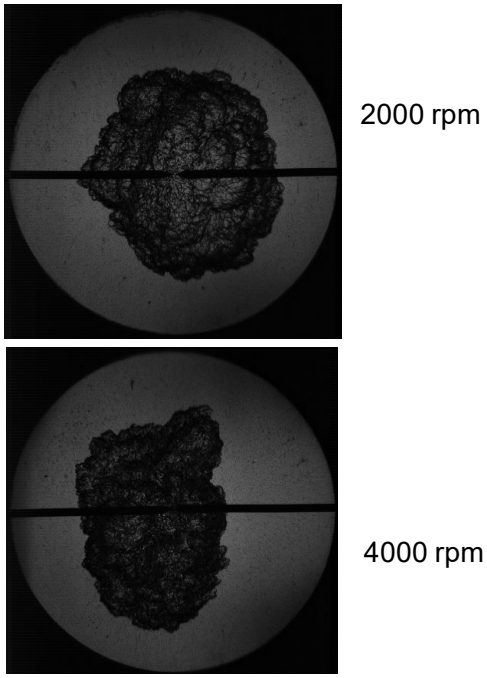

Figure 18. Typical schlieren images from the 5-bar syngas flames for two different fan speeds.

Turbulent displacement velocity of the burned gases, S_{Tb}, is obtained by numerical differentiation of the radius-versus-time curves. This procedure yields noisy derivatives, so for each run the radii history was smoothed with a Savitsky-Golay method (2^{nd} order polynomial, 10 points per window). To further reduce the data, the repetitions for each condition were then averaged. The results for all shaft speeds are presented in Fig. 22 for all three pressures (1, 5, 10 bar). An additional set of results at 2 bar and 8000 rpm is also shown in Fig. 22. The promoting effect of shaft speed on the turbulent displacement speed of the burned is again confirmed by the results in Fig. 22. However, the effect of pressure is not as straightforward and does not seem to be as strong as the effect of turbulence level/fan speed for the range of conditions tested herein.

Further study is certainly required, but the data presented in this study validate the operation of the new facility and demonstrate the type and quality of the results that can be obtained therewith. Of course, the present facility is not intended to model a typical internal flow field of a gas turbine combustor. For the reasons stated in the Introduction, its

usefulness will be borne out in the fundamental understanding to be gained, along with the data that can be used for the validation of models that can in turn be implemented for simulating gas turbine combustion processes.

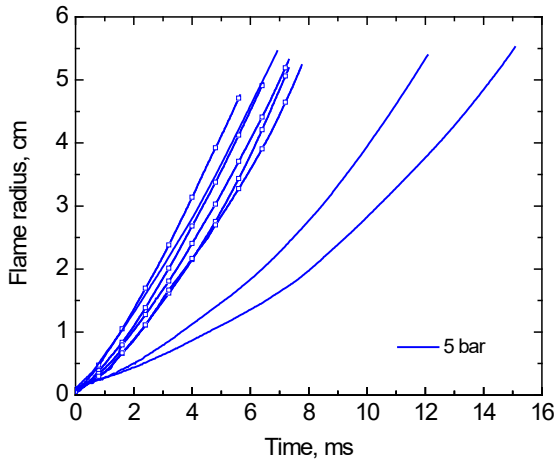

Figure 19. Radius histories of several test repetitions at 2000 and 4000 rpm and 5 bar.

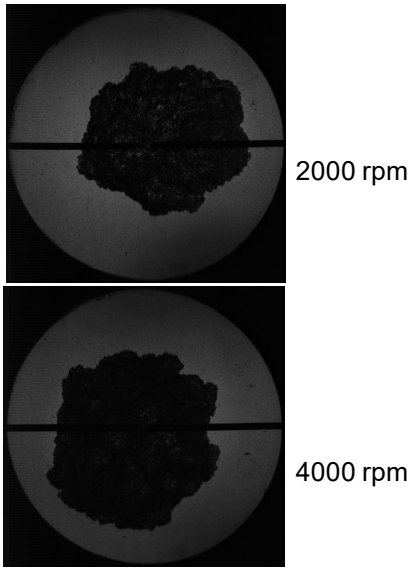

Figure 20. Typical schlieren images from the 10-bar syngas flames for two different fan speeds.

CONCLUSIONS

The need of devices capable of measuring the fundamental properties of turbulent combustion at high temperature and high pressure was identified. To the authors' knowledge, prior to this contribution there was only one fan-stirred flame bomb in the world capable of creating a turbulence fluctuation intensity higher than 5 m/s that also has access to elevated temperature and pressure. Details on the design and characterization of a new flame speed facility capable of 10 atm and 400 K were presented in this paper.

Details of key features of the new fan-stirred flame bomb were discussed. In terms of optical access, the bomb developed in this work is superior to the previous generations built by the authors' group at Texas A&M University. The new apparatus has 4 windows, each with a clear aperture of 12.7 cm (5 in) and arranged in two perpendicular lines of sight. The windows enable combustion diagnostics and flow measurement techniques that were not possible in past iterations.

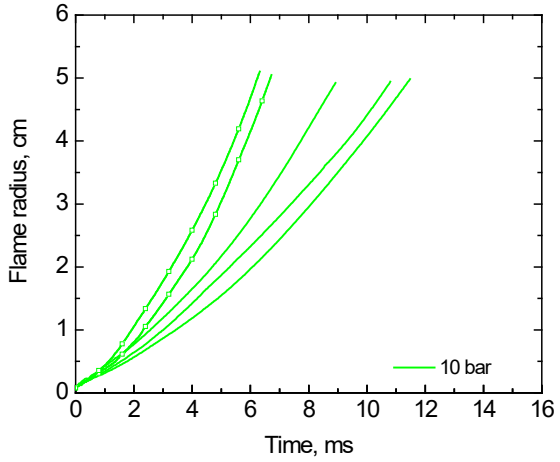

Figure 21. Radius histories of several test repetitions at 2000 and 4000 rpm and 10 bar.

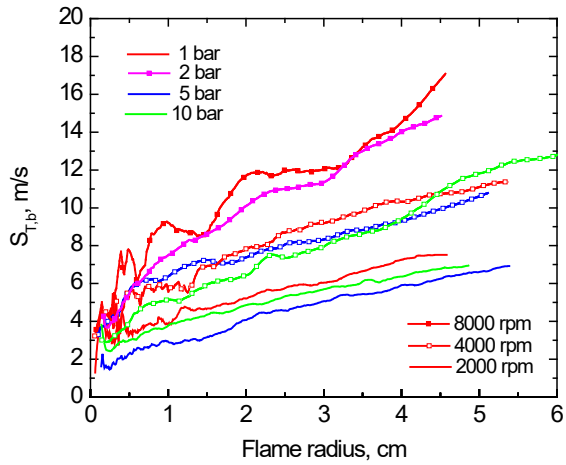

Figure 22. Displacement velocity of burned gases stirred at 2000, 4000, and 8000 rpm for all pressure levels.

The temperature operation ceiling is set by the elastomeric materials chosen for the seals. In the as-built condition, 150°C should be within reach. Safety factors are in place to test combustible mixtures at 10-bar initial pressure. The highest turbulence fluctuation rms used during the demonstration

experiments was 5.5 m/s. These are not the most demanding specifications achieved worldwide, but they are not trivial either. Furthermore, preparations were made to modify the vessel and extend the experiment domain to 20 bar by employed a vented system capability.

As a whole, the experimental setup was able to reproduce laminar flame speed benchmarks and demonstrated excellent repeatability. The vessel also showed that the entire field of view is usable without concerns of confinement. For the first time, the presence of NOx was noticed and diagnosed in a flame vessel built by the authors' team. The new experimental apparatus demonstrated procedural competence and structural integrity in a series of syngas-air turbulent flame speed experiments. The full range of pressure domain (1 – 10 bar) was exacted without issues, even at fan speeds up to 8000 rpm. General trends of the effect of turbulence were in line with expectation, but more experiments are needed to gain insight on the role of pressure.

ACKNOWLEDGMENTS

This work was made possible in part by Department Of Energy's University Turbine Systems Research program under Grant Number DE-FE0011778. Additional funding came from the National Science Foundation under Grant Number EEC-1560155 and from Siemens Canada with Dr. Gilles Bourque as project monitor.

REFERENCES

[1] Damköhler, G., 1940. "Der Einfluss der Turbulenz auf die Flammengeschwindigkeit in Gasgemischen". *Zeitschrift für Elektrochemie und angewandte physikalische Chemie*, **46**(11), pp. 601-626.

[2] Chen, J. H., 2011. "Petascale direct numerical simulation of turbulent combustion—fundamental insights towards predictive models". *Proceedings of the Combustion Institute*, **33**(1), pp. 99-123.

[3] McIlroy, A., McRae, G., Sick, V., Siebers, D. L., Westbrook, C. K., Smith, P. J., Taatjes, C., Trouve, A., Wagner, A. F., Rohlfing, E., Manley, D., Tully, F., Hilderbrandt, R., Green, W., Marceau, D., O'Neal, J., Lyday, M., Cebulski, F., Garcia, T. R., and Strong, D., 2006. "Basic Research Needs for Clean and Efficient Combustion of 21st Century Transportation Fuels". USDOE Office of Science.

[4] Pope, S. B., 2013. "Small scales, many species and the manifold challenges of turbulent combustion". *Proceedings of the Combustion Institute*, **34**(1), pp. 1-31.

[5] Abdel-Gayed, R. G., Al-Khishali, K. J., and Bradley, D., 1984. "Turbulent burning velocities and flame straining in explosions". *Proceedings of the Royal Society of London. Series A, Mathematical and physical sciences*, **391**(1801), pp. 393-414.

[6] Fansler, T. D. and Groff, E. G., 1990. "Turbulence characteristics of a fan-stirred combustion vessel". *Combustion and Flame*, **80**, pp. 350-354.

[7] Groff, E. G., 1987. "An experimental evaluation of an entrainment flame-propagation model". *Combustion and Flame*, **67**, pp. 153-162.

[8] Groff, E. G., 1982. "The cellular nature of confined spherical propane-air flames". *Combustion and Flame*, **48**, pp. 51-62.

[9] Haq, M. Z., 1998. "Fundamental Studies of Premixed Combustion". Ph.D. Thesis, The University of Leeds, Leeds, UK.

[10] Sick, V., Hartman, M. R., Arpaci, V. S., and Anderson, R. W., 2001. "Turbulent scales in a fan-stirred combustion bomb". *Combustion and Flame*, **127**, pp. 2119-2123.

[11] Smallbone, A., Tsuneyoshi, K., and Kitagawa, T., 2006. "Turbulent and stable/unstable laminar burning velocity measurements from outwardly propagating spherical hydrogen-air flames at elevated pressures". *Journal of Thermal Science and Technology*, **1**(1), pp. 31-41.

[12] Kitagawa, T., Nakahara, T., Maruyama, K., Kado, K., Hayakawa, A., and Kobayashi, S., 2008. "Turbulent burning velocity of hydrogen–air premixed propagating flames at elevated pressures". *International Journal of Hydrogen Energy*, **33**, pp. 5842-5849.

[13] Weiß, M., 2008. "Untersuchung von Flammenfront-streckungseffekten auf die sphärische Flammenausbreitung laminarer und turbulenter Brennstoff/Luft-Gemische". Ph.D. Thesis, Karslruhe Institute of Technology, Germany.

[14] Weiß, M., Zarzalis, N., and Suntz, R., 2008. "Experimental study of Markstein number effects on laminar flamelet velocity in turbulent premixed flames". *Combustion and Flame*, **154**, pp. 671–691.

[15] Liu, C. C., Shy, S. S., Chen, H. C., and Peng, M. W., 2011. "On interaction of centrally-ignited outwardly-propagating premixed flames fully-developed isotropic turbulence at elevated pressure". *Proceedings of the Combustion Institute*, **33**, pp. 1293-1299.

[16] Liu, C. C., Shy, S. S., Chiu, C. W., Peng, M. W., and Chung, H. J., 2011. "Hydrogen/carbon monoxide syngas burning rates measurements in high-pressure quiescent and turbulent environment". *International Journal of Hydrogen Energy*, **36**, pp. 8595-8603.

[17] Peng, M. W., 2010. "Measurements of Laminar and Turbulent Burning Velocities for Centrally-Ignited, Outwardly Propagation Premixed Flames at Elevated Pressure". M.S. Thesis, National Central University, Taiwan, Taiwan.

[18] Shy, S. S., I, W. K., and Lin, M. L., 2000. "A new cruciform burner and its turbulence measurements for premixed turbulent combustion study". *Experimental Thermal and Fluid Science*, **20**, pp. 105-114.

[19] Chaudhuri, S., Wu, F., and Law, C. K., 2012. "Turbulent Flame Speed Scaling for Expanding Flames with Markstein Diffusion Considerations". arXiv preprint arXiv:1203.1029.

[20] Chaudhuri, S., Wu, F., Zhu, D., and Law, C. K., 2012. "Flame Speed and Self-Similar Propagation of Expanding

Turbulent Premixed Flames". *Physical Review Letters*, **108**, p. 044503.
[21] Ravi, S., Peltier, S. J., and Petersen, E. L., 2013. "Analysis of the impact of impeller geometry on the turbulent statistics inside a fan-stirred, cylindrical flame speed vessel using PIV". *Experiments in Fluids*, **54**, p. 1424.
[22] Morones Ruelas, A., 2015. "Turbulence Measurements in a Fan-Stirred Flame Bomb Using Laser Doppler Velocimetry". M.S. Thesis, Texas A&M University, College Station, TX, USA.
[23] Galmiche, B., Mazellier, N., Halter, F., and Foucher, F., 2014. "Turbulence characterization of a high-pressure high-temperature fan-stirred combustion vessel using LDV, PIV and TR-PIV measurements". *Experiments in Fluids*, **55**, pp. 1-20.
[24] Goulier, J., Chaumeix, N., Halter, F., Meynet, N., and Bentaïb, A., 2017. "Experimental study of laminar and turbulent flame speed of a spherical flame in a fan-stirred closed vessel for hydrogen safety application". *Nuclear Engineering and Design*, **312**, pp. 214-227.
[25] Krejci, M. C., Mathieu, O., Vissotski, A. J., Ravi, S., Sikes, T. G., Petersen, E. L., Kérmonès, A., Metcalfe, W., and Curran, H. J., 2013. "Laminar Flame Speed and Ignition Delay Time Data for the Kinetic Modeling of Hydrogen and Syngas Fuel Blends". *Journal of Engineering for Gas Turbines and Power*, **135**(2), pp. 021503-021501.
[26] Morones Ruelas, A., 2018. "Study of spherical turbulent flames in a reconfigurable fan-stirred bomb". Ph.D. Thesis, Texas A&M University, August.
[27] Morones, A., León, V., and Petersen, E. L. 2017. "Reconfigurable fan-stirred flame bomb with optical access". AIAA Paper 2017-1783, AIAA SciTech Forum, 55th AIAA Aerospace Sciences Meeting, Jan. 9-13, Grapevine, TX.
[28] ASME, 2015. Section VIII Rules for Construction of Pressure Vessels, "ASME boiler and pressure vessel code," ASME.
[29] Oberg, E., Jones, F. D., Horton, H. L., and Ryffel, H. H., 2012. *Machinery's Handbook (29th Edition) & Guide to Machinery's Handbook*, Industrial Press.
[30] Clean Air Technology Center (MD-12), 1999. "Nitrogen oxides (NOx): why and how they are controlled". No. EPA-456/F-99-006R, U.S. Environmental Protection Agency, Research Triangle Park, N.C.
[31] De Vries, J., 2009. "A study on spherical expanding flame speeds of methane, ethane, and methane/ethane mixtures at elevated pressures". Ph.D. Thesis, Texas A&M University, College Station, TX.
[32] Krejci, M. C., 2012. "Development of a New Flame Speed Vessel to Measure the Effect of Steam Dilution on Laminar Flame Speeds of Syngas Fuel Blends at Elevated Pressures and Temperatures". M.S. Thesis, Texas A&M University, College Station, TX.
[33] Lefebvre, A. H. and Ballal, D. R., 2010. *Gas Turbine Combustion: Alternative Fuels and Emissions*. 3rd ed., Taylor & Francis, Boca Raton, FL.
[34] Poinsot, T. and Veynante, D., 2012. *Theoretical and Numerical Combustion*. France.